

Research Article

Zafar Mahmood, Khadija Rafique*, Ioan-Lucian Popa, Abhinav Kumar, and Mushtaq Ahmad Ansari

Rheological and irreversibility analysis of ternary nanofluid flow over an inclined radiative MHD cylinder with porous media and couple stress

<https://doi.org/10.1515/arh-2025-0050>

received June 17, 2025; accepted June 20, 2025

Abstract: This work aims to examine the influence of the shape factor on the hydrodynamic and thermal characteristics of ternary hybrid nanofluid flow over an inclined cylinder. The objective is to analyze the cumulative impacts of couple stress, porous medium, mixed convection, thermal radiation, mass suction, viscous dissipation, variable electrical conductivity, Joule heating, velocity and thermal slip conditions, and shape factor on flow dynamics, heat transfer enhancement, and entropy production. Utilize a dimensionless variable set to convert the governing partial differential equations into a system of interconnected ordinary differential equations, and then solve them numerically using the `bvp4c` function in MATLAB. The effects of dimensionless factors, including curvature parameter, porous medium, nanoparticle volume fraction, couple stress, inclination angle, mixed convection parameter, mass suction, Eckert number, Brinkmann number, thermal radiation, and magnetic parameters, are examined. The velocity profile and skin friction of various shapes (spherical, platelets, bricks, blades, cylinders)

diminish as the couple stress parameter increases. The curvature parameter exhibits dual behavior in the velocity profile, whereas the temperature profile shows an increase. Mass suction enhances the velocity profile and diminishes the temperature profile. The Eckert number elevates the temperature profile while diminishing heat transfer. Enhancing nanoparticle values diminishes skin friction and augments heat transfer. Entropy generation escalates with higher values of nanoparticle volume fraction, Brinkman number, porous media, and radiation parameters. The morphology of platelets exhibits superior velocity profiles and enhanced heat transfer relative to other shapes. The findings of this research are very consistent with those of other studies.

Keywords: shape factor, ternary hybrid nanofluid, thermal radiation, variable electrical conductivity, entropy generation, computational analysis

Nomenclature

g	Gravity acceleration (m/s^2)
v_w	Mass surface velocity (m/s)
L	Characteristic length
T	Ternary-hybrid nanofluid temperature (K)
T_∞	Ambient temperature (K)
β	Variable electrical conductivity parameter
ϕ_2	Nanoparticle volume fraction of MgO
Ec	Eckert number
S	Mass suction parameter
Cf_x	Coefficient of skin friction
Pr	Prandtl number
α_1	Temperature difference parameter
m	Shape factor
γ	Curvature parameter
λ	Stretching cylinder parameter
A	Velocity slip parameter
ε	porosity parameter
μ	Dynamic viscosity of the fluid (kg/ms)
s_2	Magnesium oxide's solid components

* **Corresponding author: Khadija Rafique**, Department of Mathematics and Statistics, Hazara University, Mansehra, Pakistan, e-mail: khadijarafique101@gmail.com

Zafar Mahmood: College of Mechanical and Vehicle Engineering, Hunan University, Changsha, Hunan, 410082, PR China

Ioan-Lucian Popa: Department of Computing, Mathematics and Electronics, "1 December 1918" University of Alba Iulia, 510009, Alba Iulia, Romania; Faculty of Mathematics and Computer Science, Transilvania University of Brasov, Iuliu Maniu Street 50, 500091, Brasov, Romania

Abhinav Kumar: Centre for Research Impact & Outcome, Chitkara University Institute of Engineering and Technology, Chitkara University, Rajpura, 140401, Punjab, India; Department of Mechanical Engineering and Renewable Energy, Technical Engineering College, The Islamic University, Najaf, Iraq

Mushtaq Ahmad Ansari: Department of Pharmacology and Toxicology, College of Pharmacy, King Saud University, P.O. Box 2457, Riyadh, 11451, Saudi Arabia

MHD	magnetohydrodynamic
Thnf	Ternary hybrid nanofluid
2D	Two-dimensional
c_p	Specific heat at constant pressure ($\text{J kg}^{-1} \text{K}^{-1}$)
ρ	Density (kg/m^3)
β_T	Thermal expansion (K^{-1})
∞	At the free stream region
u, v	Components of velocity (m/s)
c_1, c_2	Constants
T_0	Reference temperature
T_w	Surface temperature of sphere (K)
B_0	Magnetic field
ϕ_1	Nanoparticle volume fraction of Ag
ϕ_3	Nanoparticle volume fraction of Fe_3O_4
δ	Mixed convection parameter
M	Magnetic field parameter
Nu_x	Nusselt number
Br	Brinkmann number
u_e	Free stream velocity
k	Thermal conductivity of the fluid (W/mK)
ω	Angle inclination parameter
Rd	Thermal radiation parameter
B	Thermal slip parameter
Cs	Couple stress parameter
$s1$	Silver's solid components
$s3$	Iron oxide's solid components
ODEs	Ordinary differential equations
PDEs	Partial differential equations
Ψ	Stream function
ν	Kinematic viscosity ($\text{m}^2 \text{s}^{-1}$)
σ	Electrical conductivity (ω/m)
w	At wall
ψ	Shape factor sphericity

1 Introduction

The geometric configuration of nanoparticles markedly affects the viscosity and thermal conductivity of nanofluids. Because they have more surface area and contact friction, non-spherical nanoparticles like blades, platelets, or bricks often make it harder for fluids to flow than spherical nanoparticles. This is called higher viscosity. These elongated or flat geometries improve thermal conductivity by establishing more extensive percolation networks and channels for heat transmission, hence enhancing thermal performance. Spherical nanoparticles decrease viscosity while slightly enhancing heat conductivity, providing a balanced trade-off. So, picking the right form factor is important for getting the best balance between viscosity

and thermal conductivity [1]. Jiang et al. [2] described the dynamics of nanofluids influenced by thermo-capillary convection resulting from five distinct nanoparticle shapes: sphere, blade, brick, cylinder, and platelet. It was found that thermo-capillary convection was strongest in nanofluids with spherical nanoparticles and weakest in those with platelet-shaped nanoparticles. Sreenivasulu and Bhuvana Vijaya [3] investigated the influence of many features, including changing viscosity, chemical reactions, heat radiation, and the form factor of nanoparticles, on the flow of a hybrid nanofluid ($\text{H}_2\text{O} + \text{MWCNT} + \text{CuO}$) over a flat plate.

Mixed convection flow, which is used in various technical and industrial applications like heat exchangers, solar collectors, and electronic cooling systems, happens when forced and natural convection forces work together. When buoyancy effects from temperature gradients mix with externally imposed flow fields to produce complicated thermal and fluid dynamic behavior, this flow regime becomes important [4]. The Richardson number often determines whether forced or free convection is more important, which helps to understand how strong buoyancy is compared to inertial forces. Prediction of heat and mass transfer rates in systems where thermal stratification and flow recirculation may arise depends on accurate modelling of mixed convection. Ragulkumar et al. [5] used a finite difference scheme to study how free convection nanofluid moves around an upright cone while considering magnetic fields. This mathematical model investigates magnetohydrodynamic (MHD), viscous dissipation, radiation, chemical reactions, and suction/injection processes using the heat and mass flow pattern. Ragulkumar et al. [6] presented a computational methodology for analyzing the two-dimensional boundary layer heat and mass transfer of water-based nanofluids over a vertical cone permeated by porous media, incorporating heat generation/absorption, thermal radiation, chemical reactions, the Soret–Dufour number, viscous dissipation, and a magnetic field. Ramesh et al. [7] conducted modelling and calculations to investigate the mixed convective flow of $\text{ND-Co}_3\text{O}_4/\text{EG}$ hybrid nanoliquid via a vertical porous cylinder. The flow analysis and formulation include slip effects and the influences of homogeneous and heterogeneous reactions.

A new class of improved working fluids called ternary hybrid nanofluids suspends three distinct types of nanoparticles in a base fluid. The unique thermal and rheological features of the nanoparticles make this combination outperform typical and hybrid nanofluids in heat transfer. Incorporating a third kind of nanoparticle significantly enhances the fluid's stability, improves its thermal conductivity, and increases its heat retention capacity. Because of

this, it is ideal for use in biological applications, cooling technologies, and energy systems [8]. A recent study by Ullah et al. [9] investigated the heat transfer properties of nanofluids, ternary hybrids, and hybrids containing nanoparticles of copper (Cu), silver (Ag), and alumina (Al_2O_3) between two elastic spinning discs maintained at a constant distance from one another. The study evaluated how thermal radiation, a heat source, Joule heating, and Arrhenius activation energy affected the new material's flow stability and temperature equations. Incorporating the influences of melting, mixed convection, Thomson, and Troian slip, Madhukesh and Ramesh [10] compared two base liquids (kerosene/water) with ternary nanoparticle transport over a stretched vertical cylinder. Jawad et al. [11] look into the Cattaneo-Christov model of Electromagnetohydrodynamic tri-hybrid nanofluid (THNF) flow with gyrotactic microorganisms, Arrhenius activation energy, and natural convection in wedge and cone shapes. Using a medium with varying permeability, Lone et al. [12] examined three-dimensional flows of a ternary hybrid nanofluid on a stretchable sheet. They also considered heat source and thermal radiation. Although they hold significant promise, the complex interaction among particle concentration, morphology, and base fluid characteristics needs more research to fully realize their advantages. Khan et al. [13] want to understand heat transmission better, which might affect many physical processes. Researchers are studying how the tetra hybrid Tiwari and Das nanofluid models affect fluid dynamics. By studying nanoparticle-rich fluids' complicated behaviors, researchers hope to find potential uses. This study looks at how a sodium alginate-based Casson tetra hybrid nanofluid moves through porous materials and between two flat surfaces, including the effects of couple stress. The work by Madhukesh et al. [14] investigated the thermal and mass transport properties of two different forms of ternary hybrid nanofluids, using water and kerosene as the base liquids inside a vertically orientated cylinder. Their study was driven by the need to improve thermal performance in energy, industrial, and biomedical applications where flow control and thermal management are essential. The study integrated the processes of melting phenomena, heat radiation, and chemical reaction.

It is important to use thermal radiation when studying heat transfer, especially when nanofluid and ternary hybrid nanofluid flows are happening at high temperatures. The radiative heat flow, dictated by the Rosseland approximation, substantially affects the energy equation by including nonlinear phenomena that augment heat transport [15]. The synergistic interaction among numerous nanoparticles in ternary hybrid nanofluids enhances thermal conductivity,

thereby intensifying radiative heat transfer effects. Ahmad et al. [16] investigated the oblique flow and heat transfer characteristics of a micropolar ternary hybrid nanofluid across a lubricated surface, including a convective boundary condition and thermal radiation. Obalalu et al. [17] use the Galerkin-weighted residual approach to solve the modelled equations and conduct a comprehensive analysis of the energy transition to improve heat transport mechanisms in renewable energy systems using ternary nanofluid flow. The flow problem also looks at the effect of non-Fourier heat flux, multiple slips, thermal radiation, and MHDs on surfaces that are very thin. The work by Wahid et al. [18] conducted a computational investigation of the unsteady flow of a water-based ternary hybrid nanofluid (alumina, copper, and titanium dioxide) across a permeable, biaxial, shrinking sheet while accounting for the effects of heat radiation. Jamrus et al. [19] studied axisymmetric flow of a nonlinearly extending or shrinking disc using $\text{Al}_2\text{O}_3\text{-Cu-TiO}_2/\text{H}_2\text{O}$ ternary hybrid nanofluid. The study addresses convective boundary conditions and thermal radiation. Guedri et al. [20] looked into the convective flow of a two-dimensional ternary hybrid nanofluid over a nonlinear stretching sheet. Adding Brownian motion and thermophoresis to the energy and mass equations stabilizes the new composition's flow and thermal characteristics. The energy equation includes heat absorption, production, and nonlinear thermal radiation. The study by Khan et al. [21] seeks to provide an examination of irreversibility in the unsteady flow of viscous fluid across a vertical flat plate characterized by a ramping wall temperature and arbitrary wall shear stress while considering the effects of thermal radiation. The Darcy–Forchheimer and time-dependent flow of a Casson hybrid nanofluid composed of single-walled and multi-walled carbon nanotubes across a Riga plate subjected to velocity slip was studied by Senthilvaldivu et al. [22] in their study of water and glycerin. The nonlinear thermal radiation and viscous dissipation effects are included in the energy equation. The study by Khan et al. [23] seeks to investigate the impact of wall shear stress on dust-laden fluids exhibiting fluctuating flow. The analysis is conducted between two non-conducting parallel plates subjected to thermal radiation, a magnetic field, and mixed convection. The fluid flow is induced by heat transfer. Each dust particle is assumed to be uniformly dispersed and spherical within the base fluid. The perturbation solution is derived using the Poincaré–Lighthill perturbation technique. Abbas et al. [24] looked at how heat radiation affects both uniform and mixed chemical substances, along with the movement of a non-Newtonian fluid over a curved surface that expands exponentially. The study by Madhu et al. [25] investigated the effects of activation energy, quadratic, nonlinear, and linear thermal radiation on the flow of hybrid nanofluids over a cylinder.

The results show that, in comparison to linear and non-linear thermal radiation situations, quadratic thermal radiation exhibits the least uniform distribution of temperatures.

For modern energy systems, ternary hybrid nanofluids' thermal and flow characteristics are dynamic due to their electrical conductivity fluctuation. Because of the temperature-dependent conductivity and synergistic effects of several nanoparticles, ternary hybrid nanofluids exhibit complex interactions not seen in ordinary fluids. Since this variance affects the flow's electromagnetic properties, heat transfer rate, and thermal conductivity, accurate projections need extensive research [26,27]. Understanding these processes helps nanofluid-based systems perform better in cooling, energy harvesting, and electronic thermal management. Afridi *et al.* [28] performed a numerical study of entropy generation in the dissipative, unstable oscillatory flow of nanofluids, distinguished by variable electrical conductivity and magnetic heating influences. Mushahary and Ontela [29] examined how electrical conductivity variations affect the irreversibility of a couple-stress hybrid nanofluid flow in a vertical porous channel. This is quadratically mixed convective flow. Reddy *et al.* [30] concentrate on how temperature affects electrical current and top-layer nanofluid mobility. Convective heat and mass transport affect electrical conductivity, viscosity, thermo diffusion, thermal radiation, and absorption. Copper and alumina–water nanofluids fill a cylindrical annulus.

Examining entropy formation in ternary hybrid nanofluid flow is crucial for evaluating the thermodynamic efficiency of sophisticated heat transfer systems. Production of entropy, which has a significant impact on system performance, is the result of the interaction between nanoparticles, heat conduction, and viscous dissipation. Understanding these concepts reduces irreversibility's and boosts thermal efficiency, optimizing energy systems. A study by Hayat *et al.* [31] looked at how an incompressible magnetized THNF moved over a curved, porous surface. Also included are the effects of entropy formation on Darcy–Forchheimer medium and natural convection heat flow. In their study, Gireesha and Anitha [32] investigated the effects of quadratic heat radiation on convective ternary hybrid nanoliquid flow in an upright microchannel. They examine the effects on thermal performance of the Darcy-Forchheimer rule, heat source coefficient, and no-slip condition. Thermodynamic and entropy studies of oblique channel flows of ternary couple stress hybrid nanoliquids in water and couple stress hybrid nanoliquids in water were the main areas of interest for Gireesha and Anitha [33]. Their study examined the couple's stress ternary liquid by analyzing the effects of heat flow, porous

medium, buoyant force, magnetic field, and convective state. Regarding the melting point in a ternary-hybrid nanoliquid flowed under the influence of a stretched surface, Hayat *et al.* [34] conducted an investigation. Radiation, heat production, and heat dissipation make up the energy equation. The pace at which entropy is generated is studied. Hayat *et al.* [35] investigated the flow of an incompressible, magnetized, ternary nanofluid in a Darcy–Forchheimer medium, including spontaneous convection over a curved surface. These result shows that when the levels of unsteadiness and variable porosity parameters increase, entropy production improves. In response to the growing need for better heat transfer in thermal systems, Liang *et al.* [36] came up with a new way to use a ternary nanofluid to improve heat transfer efficiency and reduce entropy formation. Additionally, a constant pressure gradient, a magnetic field, Joule heating, and thermal radiation all have an impact on the flow dynamics. A study by Khan *et al.* [37] built on the concept of entropy creation in a dusty tetra hybrid nanofluid that moves freely between two vertical, parallel plates that are not moving. Both buoyant force and free convection generate the flow, which in turn transfer's heat. Ali *et al.* [38] investigated the convective flow of cross fluid containing carboxymethyl cellulose in water across a stretched sheet with convective heating. The examination investigates minimizing entropy formation. The primary objective of Anitha and Gireesha [39] work is to examine the flow characteristics and irreversibility analysis of water-based $\text{CuO-Fe}_3\text{O}_4$ hybrid nanofluid and $\text{CuO-Fe}_3\text{O}_4\text{-Ag}$ ternary hybrid nanofluid inside an inclined microchannel. The impact of the heat source coefficient, Hall current, nonlinear radiative heat flux, and slip condition on the flow of ternary nanofluid in a channel has been examined, taking into account buoyant force and the Buongiorno model.

1.1 Novelty of current research

This study is distinctive as it explores a research gap concerning the influence of shape factor on flow, heat transfer, and entropy generation of a ternary-hybrid nanofluid flowing past an inclined cylinder, incorporating couple stress, variable electrical conductivity, magnetic field, porous media, viscous dissipation, thermal radiation, velocity and thermal slip conditions, mixed convection, mass suction, and Joule heating at the stagnation point. The following research questions aims to address a gap in the literature by analyzing the effects of considering physical phenomena.

1.2 Research questions

The purpose of this study is to find the answers to the following conceptual problems.

- In ternary-hybrid nanofluids, how does the form factor (spherical, platelets, bricks, blades, cylinders) mostly influence velocity, temperature, skin friction, heat transfer, and entropy production profiles?
- How do the magnetic parameter, porous media, nanoparticle volume fraction, and mass suction influence the flow and skin friction of ternary-hybrid nanofluids with respect to form variables over an inclined cylinder?
- In a ternary hybrid nanofluid flow of different shapes over an inclined cylinder, how do thermal radiation, the Eckert number, variable electrical conductivity and the thermal slip parameter affect the temperature and heat transfer?
- What parameter optimizes entropy production and heat transfer in ternary-hybrid nanofluid?

1.3 Real-world applications

The study of the shape factor in ternary nanofluid flow over an inclined MHD radiative cylinder with porous media and coupling stress has important applications in high-tech systems that control heat. The main uses are to improve drilling and extraction processes, where heat transfer and magnetic effects inside porous rock formations are very important.

2 Problem formulation

This study examines the effects of buoyancy on the stagnation point flow of an Ag + MgO + Fe₃O₄/H₂O ternary hybrid nanofluid across an inclined cylinder in a steady, incompressible MHD mixed convection situation, as shown in Figure 1. Along the axial and radial directions of the inclined cylinder, respectively, are the coordinates (x, r) formed. The problem formulation is based on the following assumptions:

- The thermophysical characteristics of the ternary hybrid nanofluid are regarded as uniform, with the exception of electrical conductivity.
- We assume that the surface temperature of the cylinder, denoted as $T_w = T_\infty + \frac{T_0 x}{L}$, where L is the characteristic length.

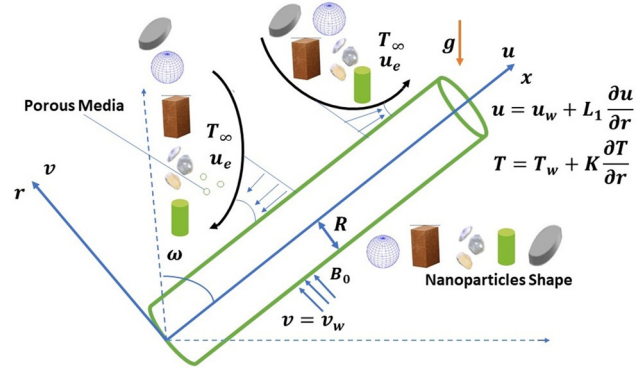


Figure 1: Physical conformation of an inclined cylinder.

- The mass transfer velocity is articulated as $v_w = -S \frac{R}{r} \sqrt{\frac{c_2 \nu_f}{L}}$, where $S > 0$ implies suction.
- The surface velocity of the cylinder is expressed as $u_w = \frac{c_2 x}{L}$, with elongation occurring when $c_2 > 0$ and contraction when $c_2 < 0$. The free stream velocity is defined as $u_e = \frac{c_1 x}{L}$, where $c_1 > 0$.
- The study incorporates Joule heating, thermal radiation, velocity and thermal slip conditions, couple stress effects, porous media, and viscous dissipation.
- The influence of nanoparticle shape factors (spherical and non-spherical) for ternary hybrid nanoparticles is included.
- Entropy generation is also considered in the analysis.

The governing equation in dimensional form appropriate for modelling the transport phenomenon is expressed as follows (see [40]):

$$\frac{\partial(ru)}{\partial x} + \frac{\partial(rv)}{\partial r} = 0, \quad (1)$$

$$\begin{aligned} u \frac{\partial u}{\partial x} + v \frac{\partial u}{\partial r} &= u_e \frac{du_e}{dx} + \frac{\mu_{\text{terhnf}}}{\rho_{\text{terhnf}}} \frac{1}{r} \frac{\partial}{\partial r} \left(r \frac{\partial u}{\partial r} \right) - \frac{\eta_0}{\rho_{\text{terhnf}}} \frac{\partial^4 u}{\partial r^4} \\ &+ (\rho\beta)_{\text{terhnf}} (T - T_\infty) g \cos \omega - \frac{\sigma_{\text{terhnf}}(T)}{\rho_{\text{terhnf}}} B_0^2 (u - u_e) \\ &- \frac{\mu_{\text{terhnf}}}{\rho_{\text{terhnf}} K_1} (u - u_e), \end{aligned} \quad (2)$$

$$\begin{aligned} u \frac{\partial T}{\partial x} + v \frac{\partial T}{\partial r} &= \frac{k_{\text{terhnf}}}{(\rho C_p)_{\text{terhnf}}} \frac{1}{r} \frac{\partial}{\partial r} \left(r \frac{\partial T}{\partial r} \right) - \frac{1}{(\rho C_p)_{\text{terhnf}}} \left(\frac{\partial q_r}{\partial r} \right) \\ &+ \frac{\sigma_{\text{terhnf}}(T)}{(\rho C_p)_{\text{terhnf}}} B_0^2 (u - u_e)^2 + \frac{\mu_{\text{terhnf}}}{(\rho C_p)_{\text{terhnf}}} \left(\frac{\partial u}{\partial r} \right)^2. \end{aligned} \quad (3)$$

The following form describes the boundary conditions (see [40]):

$$u = u_w + L_1 \frac{\partial u}{\partial r}, \frac{\partial^2 u}{\partial r^2} = 0, v = v_w, T = T_w + K \frac{\partial T}{\partial r} \text{ at } r = R,$$

$$u \rightarrow u_e, \frac{\partial u}{\partial r} \rightarrow 0, T \rightarrow T_\infty \text{ as } r \rightarrow \infty. \quad (4)$$

This research uses the variables u and v to represent the velocity components along the x -axis and r -axis, respectively. The variables g and ω stand for the gravitational acceleration and angle of inclination, respectively. B_0 is uniform magnetic field. Along with T representing the temperature of the ternary hybrid nanofluid, the parameters L_1 , K , and $K_1 = K_0 \left(\frac{x}{L} \right)$ stand for the permeability, velocity slip factor, and thermal slip factor of the porous medium, respectively.

To address the variance in electrical conductivity in the aforementioned equation, the below formula may be used (see [8]):

$$\sigma_{\text{terhnf}}(T) = \sigma_{\text{terhnf}} \left[1 + \beta \frac{T - T_\infty}{T_w - T_\infty} \right], \quad (5)$$

where β represent a positive constants.

Table 1 enumerates the thermophysical properties of the base fluid (H_2O) and the nanoparticles (Ag, MgO, and Fe_3O_4). Table 2 delineates the correlation parameters for the Ag + MgO + $\text{Fe}_3\text{O}_4/\text{H}_2\text{O}$ ternary hybrid nanofluid, including the form factor $m = 3/\psi$, with ψ denoting nanoparticle sphericity. Table 3 presents the coefficients A_1 and A_2 used in the effective viscosity model for non-spherical particles, reflecting the influence of various geometries. It also includes dynamic viscosity correlations for both spherical and non-spherical nanoparticle geometries.

For similarity solutions, the application of a similarity transformation produces the following outcomes (refer to [40]):

$$\Psi = \left(\frac{u_e \nu_f x}{L} \right)^{1/2} R f(\eta), \quad \theta(\eta) = \frac{T - T_\infty}{T_w - T_\infty},$$

$$\eta = \frac{r^2 - R^2}{2R} \sqrt{\frac{u_e}{\nu_f x L}}. \quad (6)$$

Stream function is denoted by Ψ , and $u = \frac{1}{r} \frac{\partial \Psi}{\partial r}$ and $v = -\frac{1}{r} \frac{\partial \Psi}{\partial x}$, which satisfies equation (1).

The application of the similarity variables delineated in equation (6) inherently fulfils equation (1) and converts equations (2)–(4) into the following set of ordinary differential equations (ODEs):

Table 1: Thermophysical appearance of the base liquid and Ag, MgO, Fe_3O_4 nanoparticles (see [8,12])

Properties	Ag (ϕ_1)	MgO (ϕ_2)	Fe_3O_4 (ϕ_3)	H_2O
ρ (kg/m ³)	10,500	3,560	5,180	997.1
C_p (J/kg K)	235	955	670	4,179
k (W/m K)	429	45	9.7	0.613
σ (Ω m) ⁻¹	6.3×10^7	1×10^{-6}	1×10^3	5.5×10^{-6}
β (VK)	19.7×10^{-6}	13×10^{-6}	10×10^{-6}	2.6×10^{-4}

$$\frac{\mu_{\text{terhnf}}}{\rho_{\text{terhnf}}} ((1 + 2\gamma\eta)f''' + 2\gamma f'') + f f'' + 1 - f^2$$

$$+ \frac{\beta_{\text{terhnf}}}{\rho_{\text{terhnf}}} \delta \theta \cos \omega - M \frac{\sigma_{\text{terhnf}}}{\rho_{\text{terhnf}}} [(1 + \beta\theta)(f' - 1)] \quad (7)$$

$$- \frac{\mu_{\text{terhnf}}}{\rho_{\text{terhnf}}} \varepsilon (f' - 1) - \frac{\text{Cs}}{\rho_{\text{terhnf}}} f'''' = 0,$$

$$\frac{1}{(\rho C_p)_{\text{terhnf}}} \left[(1 + 2\gamma\eta) \left(k_{\text{terhnf}} + \frac{4}{3} \text{Rd} \right) \theta' \right]$$

$$+ 2\gamma \frac{1}{(\rho C_p)_{\text{terhnf}}} \left[k_{\text{terhnf}} + \frac{4}{3} \text{Rd} \right] \theta'$$

$$+ \text{Pr} \left[(f\theta' - f'\theta) + \text{Ec} \frac{\mu_{\text{terhnf}}}{(\rho C_p)_{\text{terhnf}}} (f'')^2 \right.$$

$$\left. + \text{Ec} M \frac{\sigma_{\text{terhnf}}}{(\rho C_p)_{\text{terhnf}}} ((1 + \beta\theta)(f' - 1)^2) \right] = 0, \quad (8)$$

$$f(0) = S, \quad f'(0) = \lambda + A f''(0), f'''(0) = 0,$$

$$\theta(0) = 1 + B \theta'(0),$$

$$f'(\eta) \rightarrow 1, f''(\eta) \rightarrow 0, \theta(\eta) \rightarrow 0, \text{ as } \eta \rightarrow \infty. \quad (9)$$

In the above equations, the Prandtl number is $\text{Pr} = \frac{\mu_f C_p}{k_f}$, $M = \frac{L \sigma_f B_0^2}{\rho_f \kappa_1}$ represent the magnetic parameter,

$\gamma = \frac{1}{R} \sqrt{\frac{\nu_f L}{c_1}}$ is the curvature parameter, and ω is the angle inclination. $\text{Ec} = \frac{u_e^2}{(T_w - T_\infty)(C_p)_f} = \frac{c_1^2 x^2}{(C_p)_f \left(T_0 \frac{x^2}{l^2} \right)} = \frac{c_1^2 l^2}{(C_p)_f (T_0)}$ is the Eckert number. $\lambda = \frac{c_1}{c_2}$, where $\lambda > 0$ designates a stretched

cylinder, S is the mass suction, $\delta = \frac{\text{Gr}}{R_e^2} = \frac{g \beta_f \left(T_0 \frac{x^2}{l^2} \right)}{c_1^2 x^2 / \nu_f} = \frac{g \beta_f (T_0)}{c_1^2 l^2 / \nu_f}$ represents the mixed convection parameter. $A = L_1 \sqrt{\frac{c_2}{\nu_f}}$ is

the velocity slip parameter, $\text{Rd} = \frac{4 \sigma^* T_\infty^3}{3 k^* k_f}$ is the thermal radiation parameter and $B = K \sqrt{\frac{c_2}{\nu_f}}$ is the thermal slip

parameter, $\varepsilon = \frac{\nu_f L}{c_1 K_0}$ is the porosity parameter and $\text{Cs} = \frac{c_1 \eta_0}{\nu_f}$ is the couple stress parameter.

Table 2: Ternary hybrid nanofluid correlation properties (see [8])

Dynamic viscosity	$\mu_{\text{terhnf}} = \mu_f(1 + A_1\phi + A_2\phi^2)$, (non-spherical) $\mu_{\text{terhnf}} = \frac{\mu_f}{(1 - \phi_1)^{2.5}(1 - \phi_2)^{2.5}(1 - \phi_3)^{2.5}}$, (spherical)
Density	$\rho_{\text{terhnf}} = (1 - \phi_3)\{(1 - \phi_2)[(1 - \phi_1)\rho_f + \phi_1\rho_{s1}] + \phi_2\rho_{s2}\} + \phi_3\rho_{s3}$
Thermal conductivity	$\frac{k_{\text{terhnf}}}{k_{\text{hnf}}} = \frac{k_{s3} + (m-1)k_{\text{hnf}} - (m-1)\phi_3(k_{\text{hnf}} - k_{s3})}{k_{s3} + (m-1)k_{\text{hnf}} + \phi_3(k_{\text{hnf}} - k_{s3})}$, where, $\frac{k_{\text{hnf}}}{k_{\text{nf}}} = \frac{k_{s2} + (m-1)k_{\text{nf}} - (m-1)\phi_2(k_{\text{nf}} - k_{s2})}{k_{s2} + (m-1)k_{\text{nf}} + \phi_2(k_{\text{nf}} - k_{s2})}$, and $\frac{k_{\text{nf}}}{k_f} = \frac{k_{s1} + (m-1)k_f - (m-1)\phi_1(k_f - k_{s1})}{k_{s1} + (m-1)k_f + \phi_1(k_f - k_{s1})}$.
Heat capacity	$(\rho C_p)_{\text{terhnf}} = (1 - \phi_3)\{(1 - \phi_2)[(1 - \phi_1)(\rho C_p)_f + \phi_1(\rho C_p)_{s1}] + \phi_2(\rho C_p)_{s2}\} + \phi_3(\rho C_p)_{s3}$
Electrical conductivity	$\frac{\sigma_{\text{terhnf}}}{\sigma_{\text{hnf}}} = \frac{k_{s3} + 2\sigma_{\text{hnf}} - 2\phi_3(\sigma_{\text{hnf}} - \sigma_{s3})}{\sigma_{s3} + 2\sigma_{\text{hnf}} + \phi_3(\sigma_{\text{hnf}} - \sigma_{s3})}$, Where $\frac{\sigma_{\text{hnf}}}{\sigma_{\text{nf}}} = \frac{\sigma_{s2} + 2\sigma_{\text{nf}} - 2\phi_2(\sigma_{\text{nf}} - \sigma_{s2})}{\sigma_{s2} + 2\sigma_{\text{nf}} + \phi_2(\sigma_{\text{nf}} - \sigma_{s2})}$, and $\frac{\sigma_{\text{nf}}}{\sigma_f} = \frac{\sigma_{s1} + 2\sigma_f - 2\phi_1(\sigma_f - \sigma_{s1})}{\sigma_{s1} + 2\sigma_f + \phi_1(\sigma_f - \sigma_{s1})}$
Thermal expansion	$(\rho\beta_T)_{\text{terhnf}} = (1 - \phi_3)\{(1 - \phi_2)[(1 - \phi_1)(\rho\beta_T)_f + \phi_1(\rho\beta_T)_{s1}] + \phi_2(\rho\beta_T)_{s2}\} + \phi_3(\rho\beta_T)_{s3}$

3 Engineering quantities of interest 3.1 Entropy generation

The skin friction coefficient, which denotes flow resistance, and the local Nusselt number, which signifies the rate of heat transfer, are critical engineering metrics for assessing flow resistance and heat transfer efficiency at the surface. These quantities are represented numerically as follows:

$$C_f = \frac{\mu_{\text{terhnf}}}{\rho_f u_e^2} \left(\frac{\partial u}{\partial r} \right)_{r=R}, \quad (10)$$

$$\text{Nu}_x = -\frac{x}{k_f(T_w - T_\infty)} k_{\text{terhnf}} \left(\frac{\partial T}{\partial r} \right)_{r=R} + (q_r)_{r=R}.$$

Through similarity transformation, the aforementioned equations may be expressed as follows:

$$C_f \text{Re}_x^{1/2} = \mu_{\text{terhnf}} f''(0), \quad (11)$$

$$\text{Nu}_x \text{Re}_x^{-1/2} = -\left(\frac{K_{\text{terhnf}}}{k_f} + \frac{4}{3} \text{Rd} \right) \theta'(0),$$

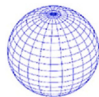




where local Reynold's number is labeled as $\text{Re}_x = \frac{u_e x}{\nu_f} = \frac{c_1 x^2}{\nu_f}$.

An important engineering metric for thermodynamic systems, including heat transmission, fluid movement, and energy dissipation, is entropy production, which measures the irreversibility. By factoring in the impacts of viscosity, Joule heating, heat conduction, and porous medium resistance, it aids in evaluating the system's efficiency (see [8,32,33,39])

$$N_s = \frac{k_{\text{terhnf}}}{T_\infty^2} \left[\left(\frac{\partial T}{\partial r} \right)^2 + \frac{16\sigma^* T_\infty^3}{3k} \left(\frac{\partial T}{\partial r} \right)^2 \right] + \frac{\sigma_{\text{terhnf}}(T)}{T_\infty} B_0^2 [(u - u_e)^2] + \frac{\mu_{\text{terhnf}}}{T_\infty} \left[\left(\frac{\partial u}{\partial r} \right)^2 \right] + \frac{\mu_{\text{terhnf}}}{K_1 T_\infty} (u - u_e)^2, \quad (12)$$

Inserting equation (6) into equation (12) yields the following outcome:

Table 3: Assessment of nanoparticle morphologies and associated coefficients for viscosity augmentation (see [8])

Nanoparticles shapes	Sphere	Bricks	Platelets	Cylinder	Blade
Shape structure					
Sphericity ψ	1	0.81	0.52	0.62	0.36
Shape factor m	3	3.7	5.7	4.8	8.6
A_1		1.9	37.1	13.5	14.6
A_2		471.4	612.6	904.4	123.3

$$N_s = \left[\alpha_1 (1 + 2\gamma\eta) \left(\frac{K_{\text{terhnf}}}{k_f} + \frac{4}{3} \text{Rd} \right) \theta'^2 \right] + \frac{\sigma_{\text{terhnf}}}{\sigma_f} M (1 + \beta\theta) (f' - 1)^2 + \frac{\mu_{\text{terhnf}}}{\mu_f} \text{Br} f'^2 + \varepsilon \text{Br} \frac{\mu_{\text{terhnf}}}{\mu_f} (f' - 1)^2, \quad (13)$$

where the Brinkmann parameters and temperature difference are quantified as follows:

$$\text{Br} = \frac{\mu_f c_1^2}{k_f (T_w - T_\infty)}, \quad \alpha_1 = \frac{(T_w - T_\infty)}{T_\infty}. \quad (14)$$

4 Numerical procedure for solution

Equations (7)–(9) were numerically resolved in MATLAB using the boundary value problem solver `bvp4c`. This solver uses the collocation formula from the three-stage Lobatto IIIa method to guarantee a continuous solution with fourth-order accuracy. An accurate initial solution estimate and an optimized boundary layer thickness for the problem parameters are the two most crucial inputs for the solver. The ‘`bvp4c`’ function in MATLAB is very beneficial for addressing boundary value issues because of its:

1. Adaptive mesh refinement automatically modifies the node distribution to meet a defined tolerance, enhancing accuracy in areas with steep slopes.
2. Proficiency in effectively managing stiff and non-linear systems, particularly prevalent in fluid mechanics and heat transfer issues represented by coupled ODEs.

We reformulated the governing equations using the system of first-order ODEs to facilitate the numerical solution. The computations were done with a tolerance error of 10^{-6} . Here are the steps that outline the process:

$$\begin{aligned} f(\eta) &= \Sigma(1); f'(\eta) = \Sigma(2); f''(\eta) = \Sigma(3); \\ f'''(\eta) &= \Sigma\Sigma1, f''''(\eta) = \Sigma\Sigma6, \end{aligned} \quad (15)$$

$$\begin{aligned} \Sigma\Sigma1 &= -\frac{\rho_{\text{terhnf}}}{\mu_{\text{terhnf}}(1 + 2\gamma\eta)} \left(2\gamma\Sigma(3) + \Sigma(1)\Sigma(3) + 1 - \Sigma(2)^2 \right. \\ &\quad + \frac{(\rho\beta)_{\text{terhnf}}}{\rho_{\text{terhnf}}} \delta\Sigma(4) \cos\omega \\ &\quad - M \frac{\sigma_{\text{terhnf}}(T)}{\rho_{\text{terhnf}}} [(1 + \beta\Sigma(4))(\Sigma(2) - 1)] \\ &\quad \left. - \varepsilon \frac{\mu_{\text{terhnf}}}{\rho_{\text{terhnf}}} (\Sigma(2) - 1) - \frac{\text{Cs}}{\rho_{\text{terhnf}}} \Sigma\Sigma6 \right], \end{aligned} \quad (16)$$

$$\theta(\eta) = \Sigma(4); \theta'(\eta) = \Sigma(5); \theta''(\eta) = \Sigma\Sigma4, \quad (17)$$

$$\begin{aligned} \Sigma\Sigma4 &= -\frac{(\rho C_p)_{\text{terhnf}}}{\left[(1 + 2\gamma\eta) \left(k_{\text{terhnf}} + \frac{4}{3} \text{Rd} \right) \right]} \left[2\gamma \frac{1}{(\rho C_p)_{\text{terhnf}}} \left(k_{\text{terhnf}} \right. \right. \\ &\quad + \frac{4}{3} \text{Rd} \left. \right) \Sigma(5) + \text{Pr} \left[\Sigma(1)\Sigma(5) - \Sigma(4)\Sigma(2) \right. \\ &\quad + \text{Ec} \frac{\mu_{\text{terhnf}}}{(\rho C_p)_{\text{terhnf}}} (\Sigma(3))^2 + \text{Ec} M \frac{\sigma_{\text{terhnf}}(T)}{(\rho C_p)_{\text{terhnf}}} (1 \\ &\quad \left. \left. + \beta\Sigma(4))(\Sigma(2) - 1)^2 \right] \right]. \end{aligned} \quad (18)$$

Table 4 presents the numerical results derived from the current investigation and juxtaposes them with the findings provided by Zainal et al. [41] and Rafique et al. [42]. This comparison validates the precision and dependability of the present computational findings by contrasting them with known data from prior investigations.

5 Results and discussion

A sequence of numerical simulations has been performed to examine the physical behavior of flow, heat transfer, and entropy formation. The results are shown via charts and tables, emphasizing the impact of different embedded factors on the governing parameter values. The following

Table 4: Comparison of the values of $f'''(0)$ and $-\theta'(0)$ with the current literature for various values of λ

λ	$f'''(0)$			$-\theta'(0)$		
	Rafique et al. [42]	Zainal et al. [41]	Present	Rafique et al. [42]	Zainal et al. [41]	Present
0.0	1.232578	1.232588	1.232588	1.1279645	1.1279644	1.1279645
0.1	1.146561	1.146560	1.146561	1.2290655	1.2290656	1.2290658
0.2	1.051130	1.051130	1.051130	1.3260932	1.3260931	1.3260933
0.5	0.713295	0.713300	0.713295	0.7132951	0.7132950	0.7132952
1.0	0.000000	0.000000	0.000000	1.9867164	1.9867165	1.9867167
2.0	-1.887307	-1.887310	-1.887307	2.6277197	2.6277196	2.6277194
5.0	-10.264749	-10.264750	-10.264749	4.0153952	4.0153953	4.0153956

are the ranges of the considered parameters: velocity slip (A): $0.0 < A \leq 1.0$, magnetic (M): $0.0 < M \leq 1.0$, mixed convection parameter (δ): $0.0 \leq \delta \leq 4.0$, mass suction (S): $1.0 \leq S \leq 2.5$, thermal slip parameter (B): $0.0 < B \leq 1.0$, Eckert number parameter (Ec): $0.0 < Ec \leq 1.0$, porous media parameter (ε): $0.0 < \varepsilon \leq 2.0$, stretching parameter ($\lambda = 0.5$), couple stress parameter (Cs): $0.5 < Cs \leq 2.5$, variable electrical conductivity parameter (β): $0.0 < \beta \leq 2.0$, nanoparticle volume fraction of Ag + MgO + Fe₃O₄/H₂O ternary hybrid nanofluid parameter (ϕ_3): $0.0 \leq \phi_3 \leq 0.03$, $\phi_1 = \phi_2 = 0.01$, angle of inclination (ω): $0^\circ < \omega \leq 90^\circ$ and $Pr = 6.2$.

Table 5 displays the numerical findings for skin friction $C_f Re_x^{1/2}$ of ternary hybrid nanofluids of various shapes (cylindrical, spherical, brick, platelet, cylinder) in relation to various technical factors.

5.1 Impact of velocity slip parameter A on $C_f Re_x^{1/2}$ of a distinct shape factor

The reduction in skin friction $C_f Re_x^{1/2}$ with a cumulative velocity slip parameter ($A = 0.1, 0.3, 0.6, 1.0$) for various nanoparticle shapes (spherical, bricks, blade, platelets, cylindrical) in an Ag + MgO + Fe₃O₄/H₂O ternary hybrid nanofluid flow arises from the interaction between slip dynamics and boundary layer modulation. Increased velocity slip reduces the near-wall velocity gradient (du/dr),

consequently decreasing shear stress ($\tau \propto \mu du/dr$) by diminishing fluid adherence. Additionally, nanoparticle morphology affects effective viscosity (μ_{terhnf}) – non-spherical shapes (bricks, platelets, cylinders) generally enhance (μ_{terhnf}) due to heightened surface interactions, whereas spherical particles reduce resistance. Still, the flattening of velocity profiles due to slip wins out over shape-induced viscous effects, which means that skin friction will steadily decrease. The synergistic thermal–rheological optimization of the ternary hybrid nanofluid mitigates viscosity extremes while maintaining this trend, while the cylinder's inclination facilitates gravitational alignment without negating the slip-driven shear reduction mechanism, underscoring the significance of boundary conditions in regulating wall shear dynamics.

5.2 Impact of couple stress parameter (Cs) on skin friction of a distinct shape factor

The decrease in skin friction $C_f Re_x^{1/2}$ magnitudes with the elevation of the couple stress parameter ($Cs = 1.0, 1.5, 2.0, 2.5$) in Ag + MgO + Fe₃O₄/H₂O ternary hybrid nanofluid flow over an inclined cylinder may be attributed to the augmented viscous relaxation effect as delineated by couple stress theory. The couple stress parameter considers non-Newtonian microstructural factors in the fluid, facilitating rotational interactions among fluid particles and

Table 5: Skin friction for various parameters values when $Pr = 6.2$, $Ec = B = Rd = 0.2$, $\delta = S = 1.0$, $\omega = 45^\circ$, $\lambda = \beta = 0.5$, $\phi_1 = \phi_2 = 0.01$, $\phi_3 = 0.02$

A	Cs	γ	ε	M	Bricks shape	Platelets shape	Cylinder shape	Blade shape	Spherical shape
0.1	1.5	0.5	0.5	0.3	1.17859	2.29244	1.96895	1.17545	0.733162
0.3	—	—	—	—	0.932324	1.81339	1.55869	0.930338	0.579752
0.6	—	—	—	—	0.70976	1.38046	1.18742	0.708602	0.441203
1.0	—	—	—	—	0.538353	1.04706	0.901151	0.537688	0.334562
0.1	1.0	—	—	—	1.18633	2.30767	1.97828	1.1816	0.738732
—	1.5	—	—	—	1.17859	2.29244	1.96895	1.17545	0.733162
—	2.0	—	—	—	1.17456	2.2845	1.96403	1.17221	0.730291
—	2.5	—	—	—	1.17208	2.27962	1.96099	1.1702	0.728539
—	1.5	0.5	—	—	1.17859	2.29244	1.96895	1.17545	0.733162
—	—	1.0	—	—	1.18637	2.30718	1.99256	1.18774	0.736151
—	—	1.5	—	—	1.19395	2.32154	2.01518	1.19956	0.739082
—	—	2.0	—	—	1.20134	2.33556	2.0369	1.21097	0.741961
—	—	0.5	0.5	—	1.17859	2.29244	1.96895	1.17545	0.733162
—	—	—	1.0	—	1.1816	2.29814	1.97806	1.1802	0.734314
—	—	—	1.5	—	1.18459	2.30381	1.98709	1.18491	0.735464
—	—	—	2.0	—	1.18757	2.30947	1.99606	1.18959	0.736611
—	—	—	0.5	0.1	1.1783	2.29187	1.96848	1.17517	0.732979
—	—	—	—	0.3	1.17859	2.29244	1.96895	1.17545	0.733162
—	—	—	—	0.6	1.17957	2.29435	1.97054	1.17641	0.733779
—	—	—	—	1.0	1.18189	2.29887	1.9743	1.17868	0.73524

diminishing the effective shear stress at the surface. As (Cs) grows, momentum diffusion inside the boundary layer diminishes, resulting in a reduced velocity gradient at the surface and subsequently lowering $C_f \text{Re}_x^{1/2}$. The inclined shape of the cylinder alters the flow behavior owing to gravitational and inertial influences, while the couple stress mechanism consistently reduces surface drag by reducing direct shear forces. This interaction leads to a general reduction in $C_f \text{Re}_x^{1/2}$ magnitudes as (Cs) rises.

5.3 Impact of curvature parameter γ on skin friction $C_f \text{Re}_x^{1/2}$ of a distinct shape factor

The intensification in $C_f \text{Re}_x^{1/2}$ magnitude with cumulative curvature parameter (γ) in Ag + MgO + Fe₃O₄/H₂O ternary hybrid nanofluid flow is attributed to enhanced flow acceleration and boundary layer compression resulting from more pronounced curvature effects. An increased γ (smaller cylinder radius in relation to boundary layer thickness) enhances the centrifugal force, resulting in a steeper velocity gradient at the wall as the fluid quickly adapts to the tighter curvature. This increases shear stress, even with the optimized viscosity of the Ag + MgO + Fe₃O₄/H₂O nanofluid resulting from synergistic interactions among nanoparticles. Curvature-driven flow acceleration also speeds up momentum diffusion next to the wall, and the inclination angle raises axial pressure gradients, which makes viscous forces stronger. Non-spherical nanoparticles, such as platelets and cylinders, contribute to this phenomenon by disrupting streamline alignment, increasing local resistance, and amplifying near-wall shear, which collectively intensify skin friction with γ .

5.4 Impact of porosity parameter ε on skin friction of distinct shape factor

The augmentation of skin friction magnitudes with elevated porous media parameter values ($\varepsilon = 0.5, 1.0, 1.5, 2.0$) in Ag + MgO + Fe₃O₄/H₂O ternary hybrid nanofluid flow over an inclined cylinder is ascribed to the increased resistance generated by the porous medium. The porous media parameter denotes the medium's permeability; as (ε) escalates, permeability diminishes, hence impeding fluid movement and intensifying the drag force inside the boundary layer. This heightened resistance amplifies the interaction between the fluid and the surface, leading to a more pronounced velocity gradient and elevated shear

stress, thus augmenting the skin friction. Moreover, the cylinder's inclination modifies the pressure and momentum distribution; nonetheless, the primary influence of decreased permeability in the porous medium exacerbates surface drag, resulting in an overall augmentation in skin friction magnitudes.

5.5 Impression of magnetic parameter M on skin friction of distinct shape factor

The augmentation of skin friction magnitudes with an increasing magnetic parameter (M) in a Ag + MgO + Fe₃O₄/H₂O ternary hybrid nanofluid flow across an inclined cylinder is ascribed to the Lorentz force produced by the applied magnetic field. An increased M amplifies this force, which counteracts fluid velocity, thus decelerating the bulk flow and compressing the boundary layer. This compression intensifies the velocity gradient at the boundary; hence, it directly increases shear stress. The magnetic field also improves the electrical conductivity of the Ag + MgO + Fe₃O₄/H₂O nanofluid, thereby integrating momentum and electromagnetic effects. Nanoparticles, particularly non-spherical forms such as platelets or cylinders, disrupt streamline alignment, thereby increasing viscous dissipation near the wall. The angle of inclination generates a gravitational component; however, the predominant resistance generated by the Lorentz force eclipses it, hence increasing drag forces. Consequently, higher M systematically augments skin friction by magnifying viscous shear and electromagnetic resistance, even though the ternary nanofluid's optimized thermal properties moderate thermal gradients.

Numerical findings of numerous important variables on the Nusselt number $\text{Nu}_x \text{Re}_x^{-1/2}$ of ternary hybrid nanofluid flow of different shapes across an inclined cylinder are shown in Table 6.

5.6 Impact of inclination angle parameter ω on Nusselt number $\text{Nu}_x \text{Re}_x^{-1/2}$ of distinct shape factor of ternary hybrid nanofluid

The augmentation of Nusselt number magnitudes with elevated inclination angle parameter ($\omega = 0^\circ, 30^\circ, 60^\circ, 90^\circ$) in Ag + MgO + Fe₃O₄/H₂O ternary hybrid nanofluid flow over an inclined cylinder is attributable to the improved convective heat transfer induced by gravitational and buoyancy forces. As the ω rises, the gravitational force

component along the cylinder surface becomes more significant, enhancing the thermal boundary layer interaction and facilitating more effective heat dissipation from the cylinder surface. The tilt alters the flow structure, resulting in a more pronounced convection-dominated regime that enhances thermal energy transfer from the surface to the adjacent fluid. This produces a more noticeable temperature differential at the surface, thereby elevating the magnitudes of the Nusselt number.

5.7 Impact of thermal slip parameter B on Nusselt number of distinct shape factor of ternary hybrid nanofluid

As the thermal slip parameter (B) goes up, the Nusselt number values go down for ternary flow over an inclined cylinder. This is because thermal slip causes the temperature gradient at the wall to go down. When (B) goes up, thermal adhesion goes down. This causes a temperature

“jump” at the boundary, which lowers the effective temperature gradient and controls conductive heat transfer. The slip-induced decoupling between the wall and fluid stops heat from moving, even though the ternary hybrid nanofluid is better at conducting heat because the nanoparticles work together to do so. The slanted cylinder design makes mixing easier because of buoyancy. However, thermal slip weakens the driving power of the thermal boundary layer, making the benefits of better conductivity less useful. Non-spherical nanoparticles (e.g., platelets, cylinders) may also disturb the near-wall region.

5.8 Impact of variable electrical conductivity parameter β on Nusselt number $Nu_x Re_x^{-1/2}$ of distinct shape factor of ternary hybrid nanofluid

The ternary hybrid nanofluid flow over an inclined cylinder exhibits a decreasing Nusselt number magnitude

Table 6: Numerical values of $Nu_x Re_x^{-1/2}$ when $Pr = 6.2$, $A = 0.1$, $S = 1.0$, $\varepsilon = \lambda = 0.5$, $M = 0.3$, $Cs = 1.5$, $\phi_1 = \phi_2 = 0.01$, $\phi_3 = 0.02$

ω	B	β	Ec	γ	δ	Rd	Bricks shape	Platelets shape	Cylinder shape	Blade shape	Spherical shape
0°	0.2	0.5	0.2	0.5	1.0	0.2	3.44388	3.59179	3.39987	3.58844	3.53049
30°	—	—	—	—	—	—	3.44389	3.59180	3.39990	3.58846	3.53051
60°	—	—	—	—	—	—	3.44391	3.59182	3.39998	3.58853	3.53053
90°	—	—	—	—	—	—	3.44394	3.59184	3.40008	3.58862	3.53056
45°	0.2	—	—	—	—	—	3.4439	3.5918	3.39994	3.58849	3.53049
—	0.5	—	—	—	—	—	1.9243	2.02008	1.90749	2.03441	1.96762
—	0.8	—	—	—	—	—	1.33517	1.40519	1.3256	1.41962	1.36387
—	1.0	—	—	—	—	—	1.10885	1.16814	1.10158	1.18157	1.13225
—	0.2	0.5	—	—	—	—	3.4439	3.5918	3.39994	3.58849	3.53049
—	—	1.0	—	—	—	—	3.44364	3.59153	3.39964	3.58818	3.53024
—	—	1.5	—	—	—	—	3.44338	3.59126	3.39934	3.58787	3.53
—	—	2.0	—	—	—	—	3.44312	3.59098	3.39905	3.58757	3.52975
—	—	0.5	0.2	—	—	—	3.4439	3.5918	3.39994	3.58849	3.53049
—	—	—	0.5	—	—	—	3.18735	3.33423	2.90772	3.15286	3.37232
—	—	—	0.8	—	—	—	2.93057	3.07644	2.41493	2.71677	3.21403
—	—	—	1.0	—	—	—	2.75927	2.90446	2.08608	2.42579	3.10844
—	—	—	0.2	0.5	—	—	3.4439	3.5918	3.39994	3.58849	3.53049
—	—	—	—	1.0	—	—	3.50851	3.66352	3.47775	3.6754	3.59001
—	—	—	—	1.5	—	—	3.57482	3.73679	3.55607	3.76257	3.65175
—	—	—	—	2.0	—	—	3.64075	3.80933	3.632801	3.84766	3.71365
—	—	—	—	0.5	1.0	—	3.4439	3.5918	3.39994	3.58849	3.53049
—	—	—	—	—	2.0	—	3.44386	3.59176	3.39978	3.58836	3.53048
—	—	—	—	—	3.0	—	3.44381	3.59172	3.39963	3.58823	3.53047
—	—	—	—	—	4.0	—	3.44377	3.59168	3.39948	3.58811	3.53046
—	—	—	—	—	1.0	0.2	3.49768	3.58717	3.39994	3.58849	3.53049
—	—	—	—	—	—	0.5	4.10355	4.18437	3.9869	4.16671	4.1462
—	—	—	—	—	—	0.8	4.65961	4.7352	4.53017	4.70505	4.70883
—	—	—	—	—	—	1.0	5.01247	5.08569	4.87667	5.04947	5.06493

as the variable electrical conductivity parameter ($\beta = 0.5, 1.0, 1.5, 2.0$) increases. This is because the fluid's thermal conductivity decreases with increasing (β). Increasing (β) causes the electrical conductivity variations in the nanofluid to reduce the fluid's effective thermal conductivity, which in turn weakens the nanofluid's heat transfer capability. So, the inclined geometry slows down the rate of convective heat transfer even more. This is because the changing flow structure makes the effect of variable conductivity stronger, which slows down the rate of convective heat transfer even more. As a result, the temperature becomes less efficient.

5.9 Impact of Eckert number parameter Ec on $Nu_x Re_x^{-1/2}$ of distinct shape factor of ternary hybrid nanofluid

When a ternary hybrid nanofluid flows over an inclined cylinder, the Nusselt number values go down as the Eckert number Ec goes up. This is because viscous dissipation effects are stronger than conductive heat transmission. An increased Ec enhances the transformation of kinetic energy into thermal energy by frictional heating, raising fluid temperatures inside the boundary layer, and reducing the temperature difference at the wall. This lowers the flow of heat that can be conducted, even though the ternary nanofluid is better at conducting heat because the nanoparticles work together to make it work better. The design of the inclined cylinder makes this tendency stronger by creating flow deceleration zones that collect viscous heating. This makes the thermal barrier layer thicker and reduces the ability to move heat. Nanoparticles that are not spherical, like platelets or cylinders, could mess up streamline coherence, which would make local dissipation worse and heat diffusion less effective. So, even though the hybrid nanofluid improves thermophysical properties, the high (Ec) causes a lot of thermal inertia, which lowers the Nusselt number. This indicates that energy retention is prioritized above heat transport between the wall and the fluid.

5.10 Impact of curvature parameter γ on the Nusselt number of distinct shape factor of ternary hybrid nanofluid

In $Ag + MgO + Fe_3O_4/H_2O$ ternary hybrid nanofluid flow, the Nusselt number magnitudes increase as the curvature parameter γ upsurges. This is mainly because the geometry's curvature effects induce an enhanced heat

transfer efficiency. The thermal boundary layer is thinner and convective heat transmission is greater when the curvature parameter is large, indicating a more prominent cylindrical shape. The heat flow is enhanced because the curvature increases the surface-to-fluid contact, which in turn increases the temperature gradient at the surface of the cylinder. The Nusselt number magnitudes are increased because the flow behavior is optimized and the heat transfer rate is further amplified by the synergy between the cylinder's inclination and curvature.

5.11 Impression of mixed convection parameter δ on the Nusselt number of distinct shape factor of ternary hybrid nanofluid

As the mixed convection parameter values ($\delta = 1.0, 2.0, 3.0, 4.0$) go up, the Nusselt number values go down. This is because buoyancy forces are stronger than forced convection effects in a ternary hybrid nanofluid flow over an inclined cylinder. As δ grows, the flow becomes more buoyancy-driven, resulting in a reduction in flow velocity near the surface and diminishing the convective heat transfer mechanism. The prevalence of natural convection impedes the dissipation of thermal energy from the cylinder's surface, resulting in a diminished temperature gradient next to the surface. As a consequence, the efficiency of heat transport diminishes, leading to reduced Nusselt number values as δ grows.

5.12 Impression of thermal radiation parameter R_d on $Nu_x Re_x^{-1/2}$ of distinct shape factor of ternary hybrid nanofluid

The $Nu_x Re_x^{-1/2}$ gets bigger in ternary $Ag + MgO + Fe_3O_4/H_2O$ nanofluid flow as the thermal radiation parameter (R_d) goes from 0.2 to 1.0. This is because the system's radiative heat transfer becomes more efficient. The net heat transfer rate from the cylinder's surface to the fluid around it rises as (R_d) grows because radiative energy exchange starts to have a bigger impact. The total efficiency of convective heat transfer is enhanced because the surface temperature gradient is amplified by this increased radiative heat flow. The effects of tilting and thermal radiation work together to make the redistribution of energy inside the boundary

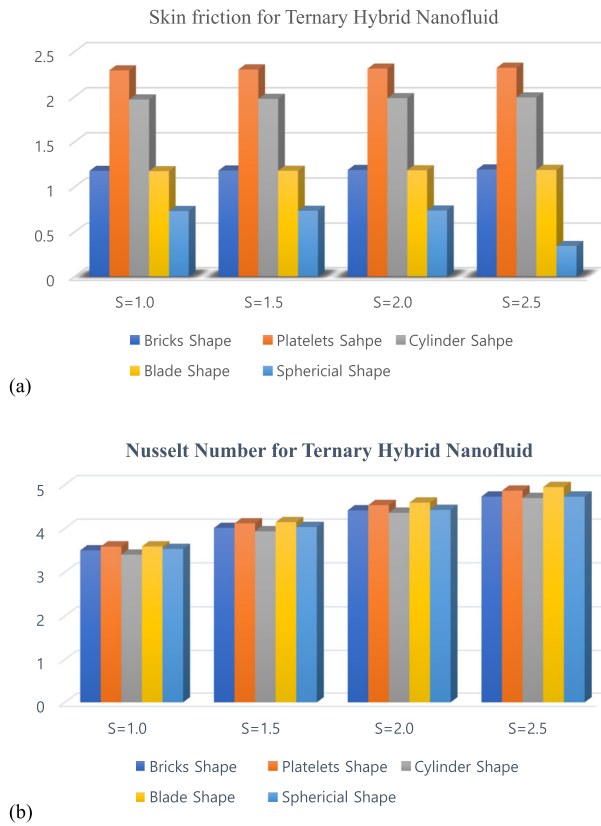


Figure 2: Impact of $S = 1.0, 1.5, 2.0, 2.5$ on (a) $C_f Re_x^{1/2}$ and (b) $Nu_x Re_x^{-1/2}$ of ternary hybrid nanofluid.

layer even better. This results in larger Nusselt numbers and a faster heat transfer rate.

Figure 2(a) and (b) validate the effect of varying mass suction parameter S on the skin friction $C_f Re_x^{1/2}$ and Nusselt number $Nu_x Re_x^{-1/2}$ of ternary hybrid nanofluid with different shape factors. Both skin friction $C_f Re_x^{1/2}$ and the

Nusselt number $Nu_x Re_x^{-1/2}$ increase with higher values of the parameter S . In ternary $Ag + MgO + Fe_3O_4/H_2O$ nanofluid flow, the $C_f Re_x^{1/2}$ and $Nu_x Re_x^{-1/2}$ both upsurge with higher values of the mass suction parameter ($S = 1.0, 1.5, 2.0, 2.5$). This is because suction influences the boundary layer dynamics, which in turn removes low-momentum fluid particles from the near-wall region, thinning the momentum and thermal boundary layers. This thinning enhances the velocity gradients at the surface, leading to higher magnitudes of skin friction. The decrease in thermal boundary layer thickness simultaneously elevates the temperature differential at the cylinder's surface, hence enhancing heat transfer and increasing the Nusselt number. The cumulative impact of these events underscores.

Figure 3(a) and (b) show how skin friction and Nusselt number over inclined cylinder vary with $Ag + MgO + Fe_3O_4/H_2O$ ternary hybrid nanofluid volume fraction ϕ_3 of a different form. These values reveal that Nusselt number rises while skin friction decreases for form factor. The decrease in skin friction and rise in Nusselt numbers that happen at the same time are caused by higher nanoparticle volume fraction parameters ($\phi_3 = 0.005, 0.01, 0.015, 0.02$) in $Ag + MgO + Fe_3O_4/H_2O$ nanofluid flow over an inclined cylinder. This is because nanoparticles have unique effects on flow and thermal properties. A higher level of ϕ_3 increases the effective viscosity of the nanofluid, which lowers the speed differences near the cylinder surface and decreases skin friction. A higher number of nanoparticles significantly improves thermal conductivity, leading to better heat transfer and a steeper temperature difference at the surface, which is indicated by a higher Nusselt number. This effect underscores the dual impact of nanoparticle volume fraction on momentum and heat transfer in the flow.

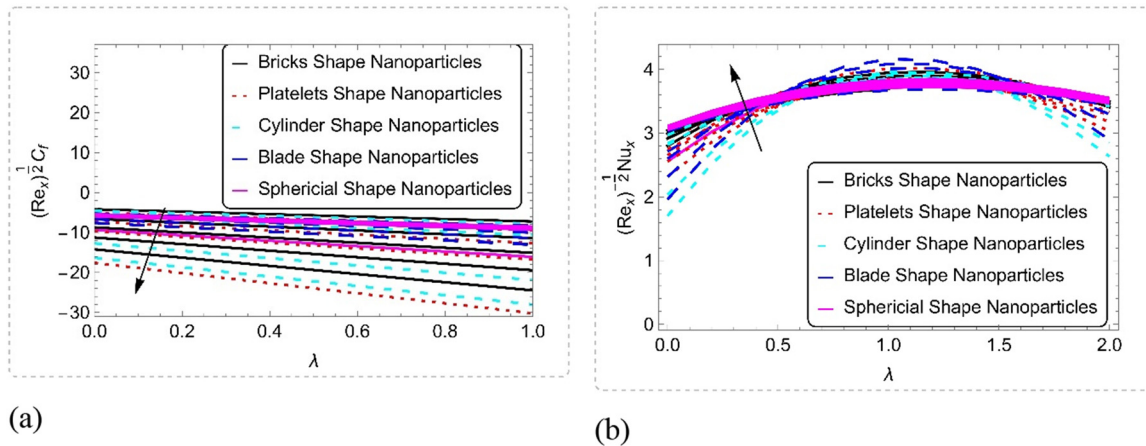


Figure 3: Influence of $\phi_3 = 0.005, 0.01, 0.015, 0.02$ on (a) $C_f Re_x^{1/2}$ and (b) $Nu_x Re_x^{-1/2}$ of distinct shape factor of ternary hybrid nanofluid.

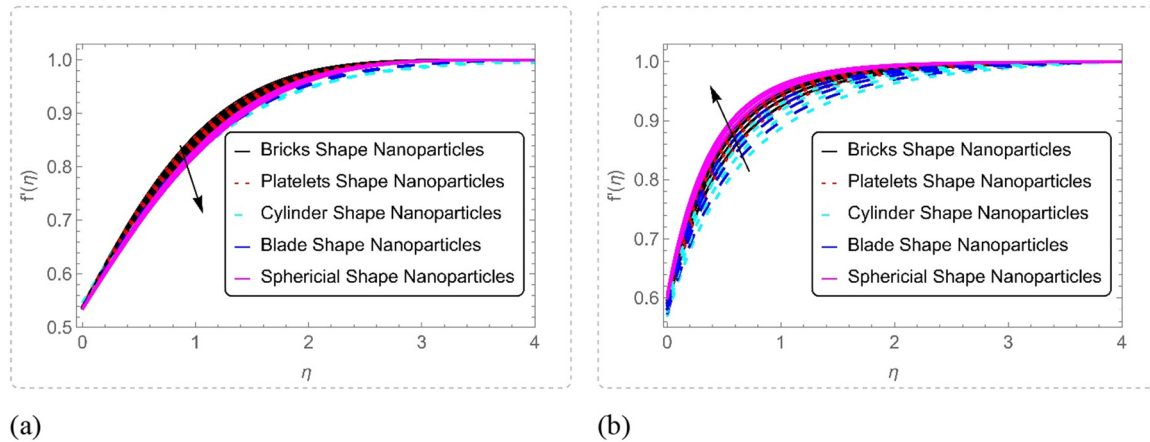


Figure 4: (a) Effect of $C_s = 1.0, 1.3, 1.5, 1.7$ on $f'(\eta)$, and (b) effect of $\epsilon = 0.5, 1.0, 1.5, 2.0$ on $f'(\eta)$.

Figure 4(a) exemplifies the consequence of the couple stress parameter (C_s) on the velocity profile $f'(\eta)$ of a $\text{Ag} + \text{MgO} + \text{Fe}_3\text{O}_4/\text{H}_2\text{O}$ ternary hybrid nanofluid with a different form, whereas Figure 4(b) shows the effect of the porous media parameter (ϵ) on the same profile. The $f'(\eta)$ profile of a $\text{Ag} + \text{MgO} + \text{Fe}_3\text{O}_4/\text{H}_2\text{O}$ nanofluid moving across an inclined cylinder shows unique features that are affected by changing the coupling stress and the parameters of the porous medium. The $f'(\eta)$ profile gets flatter as the couple stress parameter ($C_s = 1.0, 1.3, 1.5, 1.7$) goes up. This is because higher couple stress increases resistance in the fluid, which is caused by microstructural interactions inside the fluid that stop it from moving. In contrast, the $f'(\eta)$ profile rises as the values of the porous media parameter ($\epsilon = 0.5, 1.0, 1.5, 2.0$) climb. This is because the porous medium experiences less drag resistance, leading to increased permeability and smoother flow. This two-pronged effect highlights the complementary roles of pair stress and porous medium in controlling the fluid's momentum transfer.

5.13 Effect of curvature parameter γ on velocity $f'(\eta)$ and temperature $\theta(\eta)$ profiles of distinct shape ternary hybrid nanofluid

Figure 5(a) and (b) exhibit the impact of the parameter (γ) on the velocity $f'(\eta)$ and temperature $\theta(\eta)$ profiles of $\text{Ag} + \text{MgO} + \text{Fe}_3\text{O}_4/\text{H}_2\text{O}$ ternary hybrid nanofluid flow across inclined cylinders of different forms. While Figure 5(b) shows the same patterns at all levels of curvature, Figure 5(a) shows the dual behavior. The $f'(\eta)$ profile of $\text{Ag} + \text{MgO} + \text{Fe}_3\text{O}_4/\text{H}_2\text{O}$ nanofluid flow over an inclined cylinder demonstrates dual behavior with increasing parameter ($\gamma = 0.5, 1.0, 1.5, 2.0$). As curvature rises, $f'(\eta)$ decreases due to centripetal pressures and physical restrictions that impede fluid motion. Surface momentum transfer and $f'(\eta)$ rise when fluid flow matches geometry at higher curvature levels. Concurrently, as the

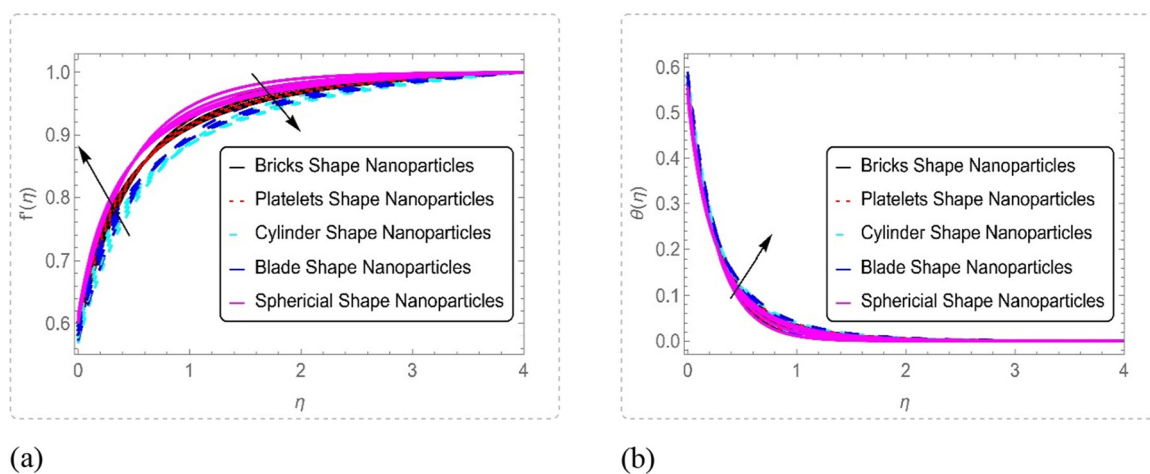


Figure 5: Impression of $\gamma = 0.5, 1.0, 1.5, 2.0$ on (a) $f'(\eta)$ and (b) $\theta(\eta)$.

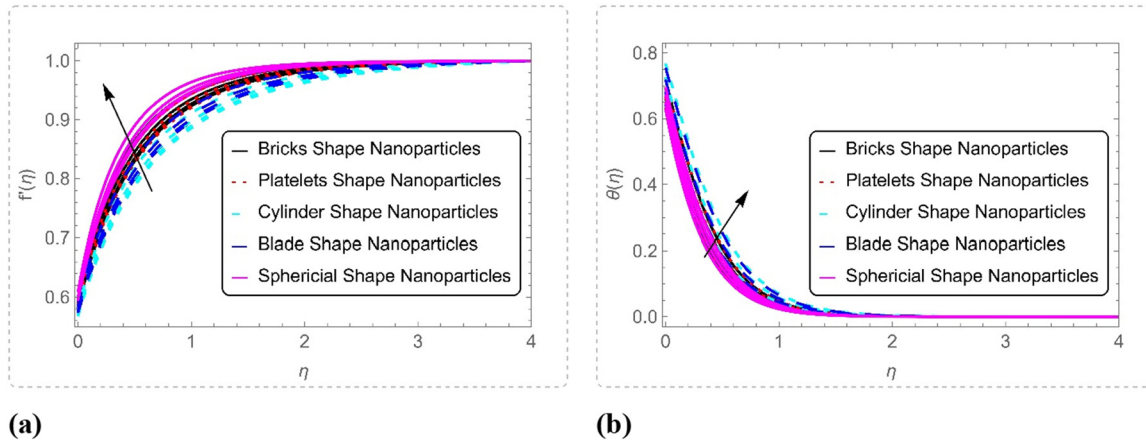


Figure 6: (a) Impression of $M = 0.1, 0.3, 0.5, 0.7$ on $f'(\eta)$, and (b) impression of $Ec = 0.1, 0.3, 0.5, 0.7$ on $\theta(\eta)$.

curvature increases, the $\theta(\eta)$ profile rises. This is because a higher curvature allows the thermal boundary layer to expand, which in turn improves the heat conduction from the surface to the fluid. Both effects show how fluid dynamics and thermal behavior interact intricately in curved geometries.

5.14 Consequence of magnetic parameter M on $f'(\eta)$ and Eckert number Ec on $\theta(\eta)$ profiles of distinct shape ternary hybrid nanofluid

Figure 6(a) demonstrates the influence of the magnetic parameter (M) on the velocity $f'(\eta)$ profile, whereas Figure 6(b) shows the effect of the (Ec) on the temperature

$\theta(\eta)$ profile of ternary $Ag + MgO + Fe_3O_4/H_2O$ nanofluid flow with different shapes of nanoparticles. As the parameter values ($M = 0.1, 0.3, 0.5, 0.7$) increase, the $f'(\eta)$ profile of the $Ag + MgO + Fe_3O_4/H_2O$ nanofluid flow over an inclined cylinder becomes steeper. This is because the magnetic field produces a Lorentz force, which acts as a driving force, propelling the fluid in the direction of flow. In contrast, the $\theta(\eta)$ profile increases with higher Eckert number values ($Ec = 0.1, 0.3, 0.5, 0.7$), as the Eckert number represents the conversion of kinetic energy into thermal energy through viscous dissipation, which enhances the fluid's thermal energy and raises its temperature. These findings highlight the combined effect of electromagnetic forces and viscous dissipation on the fluid and thermal dynamics inside the system.

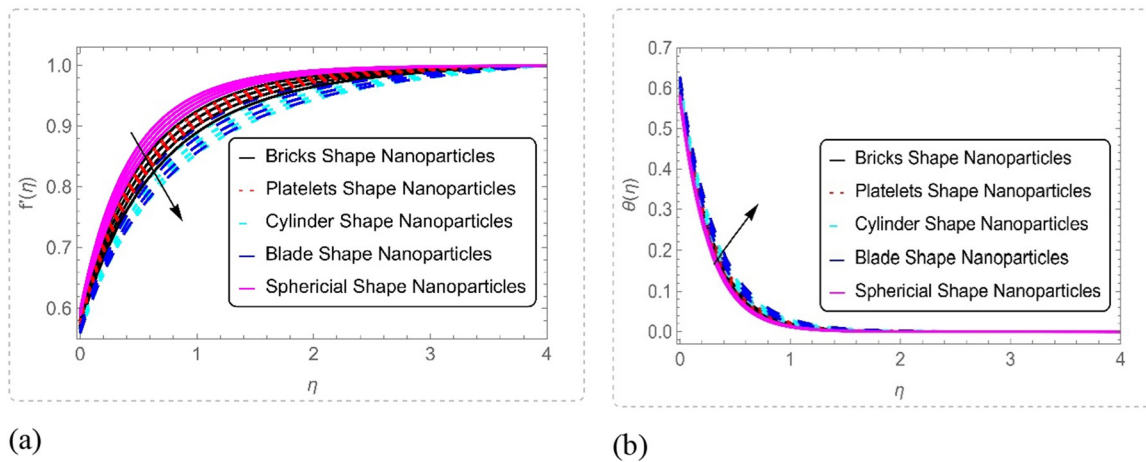


Figure 7: Impression of $\phi_3 = 0.005, 0.01, 0.015, 0.02$ on (a) $f'(\eta)$ and (b) $\theta(\eta)$.

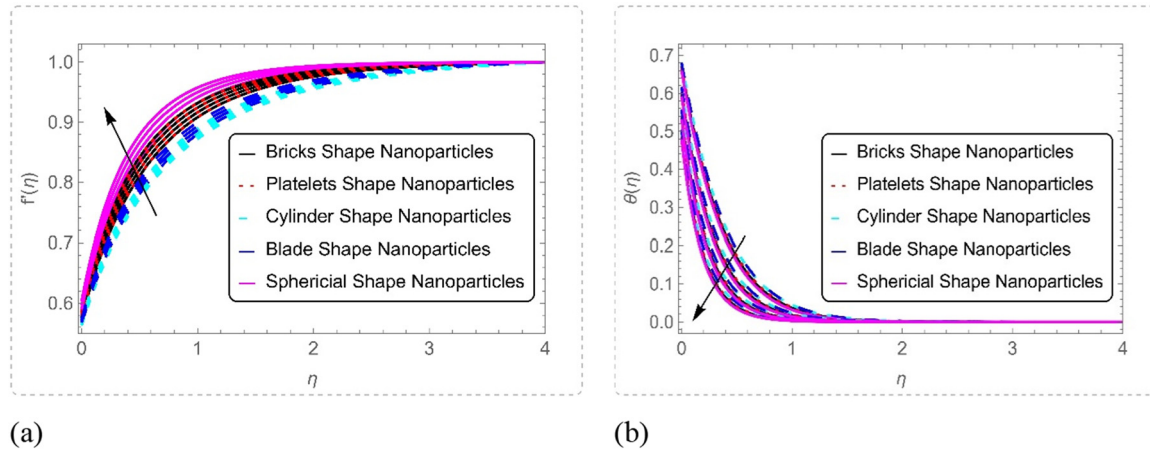


Figure 8: Impact of $S = 1.0, 1.5, 2.0, 2.5$ on (a) $f'(\eta)$ and (b) $\theta(\eta)$.

5.15 Effect of nanoparticle volume fraction (ϕ_3) on velocity $f'(\eta)$ and temperature $\theta(\eta)$ profiles of distinct shape factor

Figure 7(a) and (b) portray the stimulus of the nanoparticle volume fraction (ϕ_3) on the velocity $f'(\eta)$ and temperature $\theta(\eta)$ profiles of an Ag + MgO + Fe₃O₄/H₂O ternary hybrid nanofluid traversing an inclined cylinder of various geometries. Rising parameters ($\phi_3 = 0.005, 0.01, 0.015, 0.02$) cause the $f'(\eta)$ profile of Ag + MgO + Fe₃O₄/H₂O nanofluid flow over an inclined cylinder to decrease. This is because the ternary nanofluid's increased density and viscosity increase flow resistance and decrease fluid velocity. Conversely, the temperature $\theta(\eta)$ profile increases with higher nanoparticle volume fractions, as the addition of nanoparticles enhances the fluid's thermal conductivity, leading to improved heat transfer and a more uniform distribution of thermal energy within the system. The interplay between

momentum and thermal transport demonstrates the dual role of nanoparticles in altering fluid dynamics and heat transfer characteristics.

5.16 Effect of mass suction parameter (S) on velocity $f'(\eta)$ and temperature $\theta(\eta)$ profiles of distinct shape ternary hybrid nanofluid

The impact of the mass suction parameter (S) on the velocity $f'(\eta)$ and temperature $\theta(\eta)$ profiles of the Ag + MgO + Fe₃O₄/H₂O ternary hybrid nanofluid is shown in Figure 8(a) and (b). In Ag + MgO + Fe₃O₄/H₂O nanofluid flow over an inclined cylinder, the $f'(\eta)$ profile increases with higher mass suction parameter values ($S = 1.0, 1.5, 2.0, 2.5$). Eliminating slower fluid layers near the surface decreases

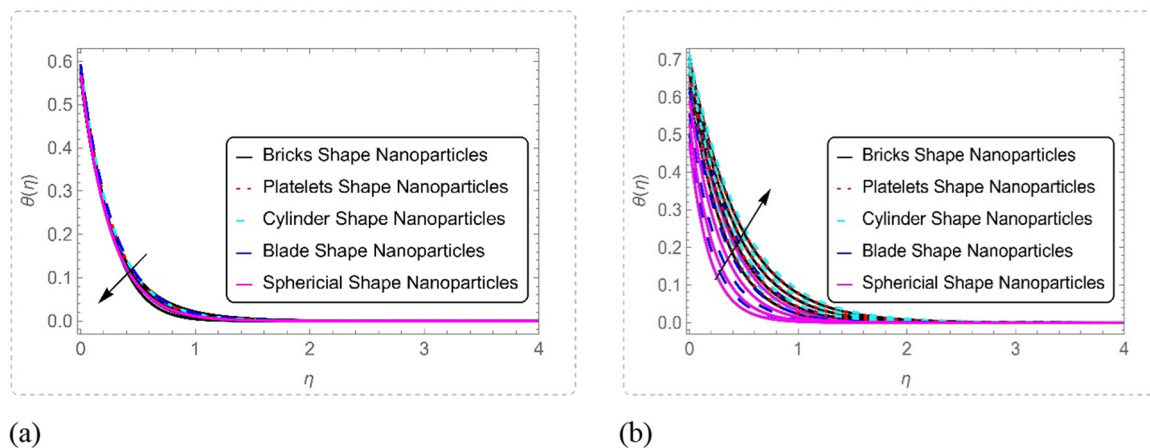


Figure 9: (a) Bearing of $\delta = 0.5, 1.0, 1.5, 2.0$ on $\theta(\eta)$, and (b) bearing of $Rd = 0.2, 0.4, 0.6, 0.8$ on $\theta(\eta)$.

boundary layer thickness and boosts momentum transfer. As suction rises, fluid evacuation lowers thermal boundary layer thickness, resulting in a drop in $\theta(\eta)$ profile. Because less heat can build up at the surface, the temperature gradient steepens, lowering fluid temperatures. This shows that suction significantly alters thermal boundary layers and momentum.

5.17 Effect of mixed convection parameter (δ) and radiation on temperature profiles of distinct shape ternary hybrid nanofluid

Both Figure 9(a) and (b) show how the mixed convection parameter (δ) and the thermal radiation parameter (Rd) affect the temperature profile of the Ag + MgO + Fe₃O₄/H₂O ternary hybrid nanofluid, respectively. The temperature distribution of a ternary hybrid nanofluid traversing an inclined cylinder diminishes as the mixed convection

parameter ($\delta = 1.0, 1.5, 2.0, 2.5$) increases. Buoyancy-driven convective cooling facilitates the dissipation of heat from the surface. At values of Rd = 0.2, 0.5, 0.7, and 1.0, the temperature profile rises with increasing thermal radiation. Radiation increases the total thermal energy inside the boundary layer by energizing the fluid. The interplay between convection-driven cooling and radiation-induced heating highlights how these two processes affect the thermal dynamics of the system in different ways.

Figure 10 displays the effects of several parameters on the generation of entropy for ternary hybrid nanofluids of different shapes over an inclined cylinder. Figure 10(a) shows the effects of the Brinkmann number parameter (Br), Figure 10(b) shows the effects of the porous media parameter (ϵ), Figure 10(c) shows the effects of the nanoparticle volume fraction parameter (ϕ_3), and Figure 10(d) shows the effects of the radiation parameter (Rd). The entropy generation profile of ternary hybrid nanofluid flow over an inclined cylinder escalates with elevated values of the (Br), (ϵ), (ϕ_3), and parameter (Rd). An elevation in (Br) indicates augmented viscous dissipation effects, thereby directly enhancing

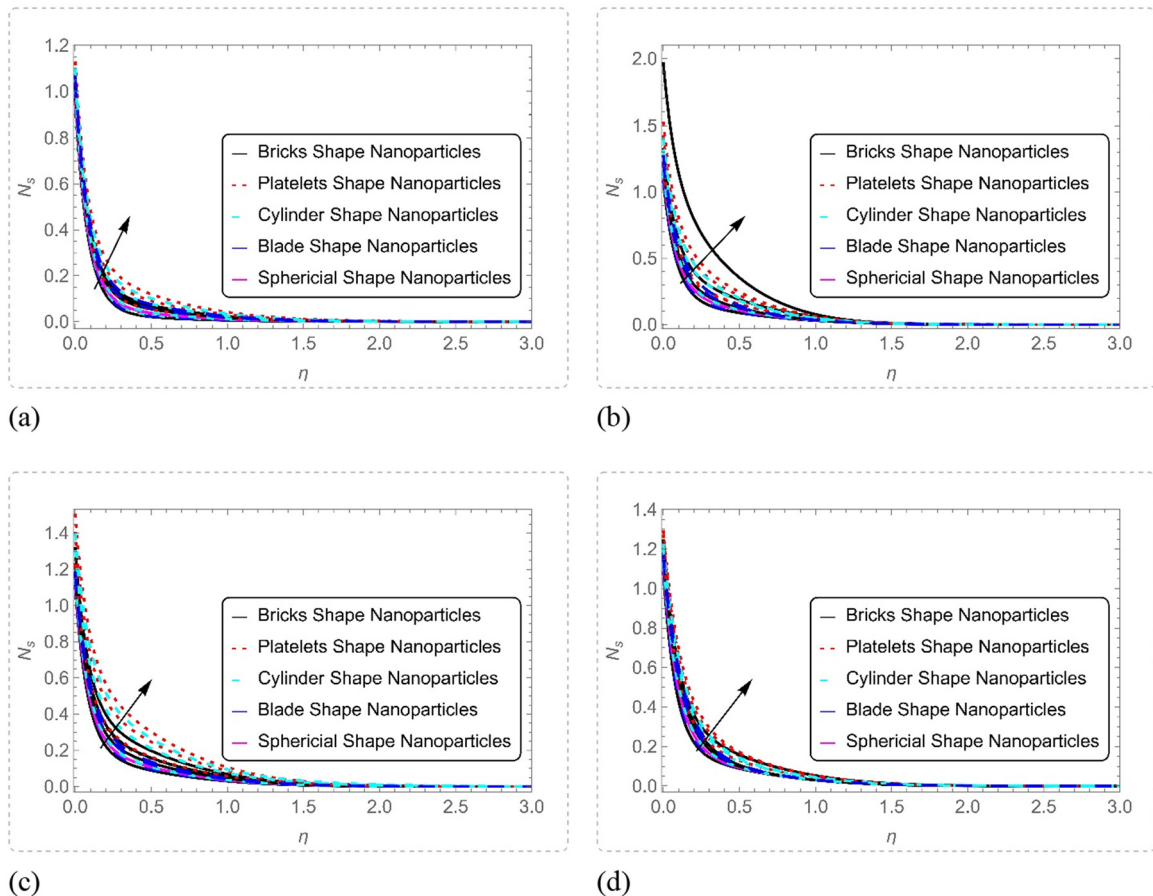


Figure 10: (a) Impact of Br = 0.2, 0.4, 0.6, 0.8 on N_s , (b) impact of $\epsilon = 0.5, 1.0, 1.5, 2.0$ on N_s , (c) impact of $\phi_3 = 0.005, 0.01, 0.015, 0.02$ on N_s , and (d) impact of Rd = 0.2, 0.4, 0.6, 0.8 on N_s .

thermal irreversibilities within the system. Likewise, an increase in (ϵ) amplifies flow resistance inside the porous medium, resulting in heightened frictional entropy formation. Increased nanoparticle volume fractions (ϕ_3) enhance thermal conductivity, thereby elevating heat transfer rates and subsequently increasing entropy production. Furthermore, an augmentation in (R_d) enhances radiative heat flux, resulting in greater temperature gradients that further facilitate entropy generation. The cumulative effect highlights the preeminence of viscous, thermal, and radiative irreversibility's within the flow system.

5.18 Significance of shape factors (bricks, platelets, cylinders, blades, spheres) on different profiles of Ag + MgO + Fe₃O₄/H₂O ternary hybrid nanofluid

The impression of shape factors (bricks, platelets, cylinders, blades, spheres) on the flow profiles of Ag + MgO + Fe₃O₄/H₂O ternary hybrid nanofluids arises from the unique hydrodynamic and thermal properties of each shape. Spherical nanoparticles exhibit minimal drag due to their symmetrical geometry, facilitating higher velocity profiles than other shapes. Blade-shaped nanoparticles, possessing a greater surface area-to-volume ratio, significantly improve heat transfer efficiency, yielding the highest Nusselt number. Platelets, with their extensive contact area and increased flow resistance, result in heightened skin friction and greater entropy generation due to marked frictional and thermal irreversibility's. This behavior underscores the intricate relationship between nanoparticle shape, flow dynamics, and heat transfer mechanisms, emphasizing the critical role of shape factors in enhancing the efficacy of nanofluid systems.

6 Conclusions

This work examined the behavior of mixed convection stagnation point flow of Ag + MgO + Fe₃O₄/H₂O ternary hybrid nanofluid across an inclined cylinder. The influence of magnetic fields, porous media, coupling stress, velocity and thermal slip conditions, mass suction, viscosity dissipation, Joule heating, variable electrical conductivity, form factor, and thermal radiation. We numerically calculated and visually and tabulatively displayed the impacts of the dimensionless parameters on the entropy production, skin friction coefficient, and heat transfer rate at the surface. The following is a list of the summary findings:

- The influence of shape factor on the flow of Ag + MgO + Fe₃O₄/H₂O ternary hybrid nanofluids across an inclined cylinder is examined, revealing that platelet shapes surpass other geometries for Nusselt number and velocity profiles.
- The velocity profile of Ag + MgO + Fe₃O₄/H₂O ternary hybrid nanofluid flow with varying form factors diminishes as the coupling stress and nanoparticle volume fraction parameters grow, whereas the velocity profile enhances with rising mass suction, magnetic, and porous medium parameters. The curvature parameter exhibits dual behavior in the velocity profile.
- The temperature profile of Ag + MgO + Fe₃O₄/H₂O ternary hybrid nanofluid flow with varying shapes diminishes with elevated mixed convection and mass suction parameters, while it increases with higher values of radiation, Eckert number, curvature, and nanoparticle volume fraction parameters.
- An Ag + MgO + Fe₃O₄/H₂O nanofluid flow with different shaped components has an entropy generation profile that grows as the Brinkmann number, porous media, nanoparticle volume percentage, and thermal radiation parameters rise.
- The skin friction of Ag + MgO + Fe₃O₄/H₂O nanofluid flow with varying morphologies escalates with higher mass suction, curvature, porous medium, and magnetic parameters, while it diminishes with rising velocity slip parameter, coupling stress, and nanoparticle volume fraction parameters.
- An Ag + MgO + Fe₃O₄/H₂O nanofluid flow with different shapes has an increasing Nusselt number for large values of mass suction, inclination angle, nanoparticle volume fraction, curvature, and radiation parameter, and a decreasing value for large values of thermal slip, Eckert number, mixed convection, and variable electrical conductivity.

7 Future suggestions

Subsequent investigations may expand upon this work by

1. Examining the effects of time-dependent flow and transient heat transfer in analogous systems to investigate unsteady-state behavior.
2. Examining various geometries, including conical and elliptical surfaces, to evaluate the influence of form on heat transport and entropy creation.
3. Integrating hybrid heating methods, like variable surface heating or non-uniform magnetic fields, to improve thermal efficiency.

4. Investigating the interplay of chemical processes or phase change events in the ternary hybrid nanofluid to enhance industrial application.
5. Making use of optimization or machine learning methods to predict the right form parameters and fluid properties to improve heat transport and decrease entropy generation.

Acknowledgments: The authors acknowledge and appreciate the Ongoing Research Funding Program (ORF-2025-996), King Saud University, Riyadh, Saudi Arabia.

Funding information: This research was supported by the Ongoing Research Funding Program (ORF-2025-996) at King Saud University in Riyadh, Saudi Arabia.

Author contributions: Z. M. and K. R.: conceptualization, methodology, software, formal analysis, validation, and writing – original draft. I. L. P.: writing – original draft, investigation, visualization, data curation, and validation. A. K.: conceptualization, writing – original draft, and formal analysis and resources. M. A. A.: supervision, validation, methodology, project administration, investigation, writing – review and editing, and software.

Conflict of interest: The authors state no conflict of interest.

Ethical approval: The conducted research is not related to either human or animals use.

Data availability statement: The datasets generated during and/or analyzed during the current study are available from the corresponding author on reasonable request.

References

- [1] Asif Ali Shah S, Kanwal S, Idrees M, Mahmood A, Mahmood I, Akgul A, et al. Significance of heat transfer rate in water-based nanoparticles with magnetic and shape factors effects: Tiwari and Das model. *Sci Rep.* 2023;13(1):15507.
- [2] Jiang Y, Zhou X, Wang Y. Effects of nanoparticle shapes on heat and mass transfer of nanofluid thermocapillary convection around a gas bubble. *Microgravity Sci Technol.* 2020;32:167–77.
- [3] Sreenivasulu M, Bhuvana Vijaya R. Influence of exponential heat source, variable viscosity and shape factor on a hybrid nanofluid flow over a flat plate when thermal radiation and chemical reaction are significant. *Mod Phys Lett B.* 2024;38(14):2450102.
- [4] Aslam MN, Shaheen A, Riaz A, Alshaikey S, Shaukat N, Aslam MW, et al. An ANN-PSO approach for mixed convection flow in an inclined tube with ciliary motion of Jeffrey six constant fluid. *Case Stud Therm Eng.* 2023;52:103740.
- [5] Ragulkumar E, Palani G, Sambath P, Chamkha AJ. Dissipative MHD free convective nanofluid flow past a vertical cone under radiative chemical reaction with mass flux. *Sci Rep.* 2023;13(1):2878.
- [6] Ragulkumar E, Sambath P, Suresh K, Balasubramanian S, Chamkha AJ. Soret–Dufour mass transfer effects on radiative chemically dissipative MHD plain convective water nanofluid (Al_2O_3 , Cu, Ag, & TiO_2) flow across a temperature-controlled upright cone surface with heat blow/suction. *Numer Heat Transf Part A Appl.* 2025;86(2):278–96.
- [7] Ramesh GK, Manjunatha S, Roopa GS, Chamkha AJ. Hybrid (ND- Co_3O_4 /EG) nanoliquid through a permeable cylinder under homogeneous-heterogeneous reactions and slip effects. *J Therm Anal Calorim.* 2021;146:1347–57.
- [8] Mahmood Z, Rafique K, Abd-Elmonem A, Suoliman NAA, Kumar A, Mukalazi H. Analyzing thermal performance and entropy generation in time-dependent buoyancy flow of water-based over rotating sphere with ternary nanoparticle shape factor. *J Comput Des Eng.* 2025;12(1):80–99.
- [9] Ullah H, Abas SA, Fiza M, Jan AU, Akgul A, Abd El-Rahman M, et al. Thermal radiation effects of ternary hybrid nanofluid flow in the activation energy: Numerical computational approach. *Results Eng.* 2025;25:104062.
- [10] Madhukesh JK, Ramesh GK. Effectiveness of kerosene/water conveying ternary ($\text{Cu-SiO}_2\text{-Al}_2\text{O}_3$) nanoparticles flowing in vertical cylinder subjected to a melting phenomenon. *J Taibah Univ Sci.* 2025;19(1):2466870.
- [11] Jawad M, Fu Z, Khan H, Ali M, Khan WA, Abu-Jrai A, et al. Bio-convection in tri-hybrid nanofluid flow with Arrhenius activation energy: Incorporating the Cattaneo-Christov heat flux model. *J Radiat Res Appl Sci.* 2025;18(1):101296.
- [12] Lone SA, AL-Essa LA, Alduais FS, Al-Bossly A, Dawar A, Saeed A. Optimization of heat transfer in bi-directional flow of sodium alginate-based ternary hybrid nanofluid over an extending heated surface with velocity slip conditions. *J Therm Anal Calorim.* 2025;150:1–12.
- [13] Khan D, Kumam P, Suttiarporn P, Srisurat T. Fourier's and Fick's laws analysis of couple stress MHD sodium alginate based Casson tetra hybrid nanofluid along with porous medium and two parallel plates. *South Afr J Chem Eng.* 2024;47:279–90.
- [14] Madhukesh JK, Ramesh GK, Revadakundi YB. Thermal transport analysis of ternary hybrid nanofluid flow over a vertical cylinder with thermal radiation and chemical reaction. *Therm Adv.* 2025;3:100040.
- [15] Ali NB, Mahmood Z, Rafique K, Khan U, Adnan, Muhammad T, et al. Exploring concentration-dependent transport properties on an unsteady Riga plate by incorporating thermal radiation with activation energy and gyrotactic microorganisms. *Appl Rheol.* 2024;34(1):20240019.
- [16] Ahmad S, Khan AA, Alkarni S. Novel insight of thermal radiation and slip boundary condition on the micropolar ternary hybrid nanofluid flow over an oblique stagnation region of a lubricated surface. *Mod Phys Lett B.* 2024;39:2550101.
- [17] Obalalu AM, Fatunmbi EO, Alam MM, Abbas A, Khan U, Adekoya-Olowofela A, et al. Influence of thermal radiation and electromagnetic characteristics of micropolar ternary hybrid nanofluid flow over a slender surface. *J Radiat Res Appl Sci.* 2025;18(1):101268.

- [18] Wahid NS, Arifin NM, Yahaya RI, Khashi'ie NS, Pop I. Impact of suction and thermal radiation on unsteady ternary hybrid nanofluid flow over a biaxial shrinking sheet. *Alex Eng J.* 2024;96:132–41.
- [19] Jamrus FN, Ishak A, Waini I, Khan U. Radiative influence on axisymmetric ternary hybrid nanofluid flow with convective boundary conditions over a nonlinearly permeable stretching/shrinking disk. *Int J Numer Methods Heat Fluid Flow.* 2024;34(12):4333–61.
- [20] Guedri K, Khan A, Sene N, Raizah Z, Saeed A, Galal AM. Thermal flow for radiative ternary hybrid nanofluid over nonlinear stretching sheet subject to Darcy–Forchheimer phenomenon. *Math Probl Eng.* 2022;2022(1):3429439.
- [21] Khan A, Ul Karim F, Khan I, Ali F, Khan D. Irreversibility analysis in unsteady flow over a vertical plate with arbitrary wall shear stress and ramped wall temperature. *Results Phys.* 2018;8:1283–90.
- [22] Senthilvadivu K, Eswaramoorthi S, Loganathan K, Abbas M. Time-dependent Darcy–Forchheimer flow of Casson hybrid nanofluid comprising the CNTs through a Riga plate with nonlinear thermal radiation and viscous dissipation. *Nanotechnol Rev.* 2024;13(1):20230202.
- [23] Khan D, Rahman AU, Ali G, Kumam P, Kaewkhao A, Khan I. The effect of wall shear stress on two phase fluctuating flow of dusty fluids by using light hill technique. *Water.* 2021;13(11):1587.
- [24] Abbas MS, Shaheen A, Abbas N, Shatanawi W. Dynamic analysis of radiative chemical species with non-Newtonian fluid flow over an exponentially curved stretching sheet. *Proc Inst Mech Eng Part E J Process Mech Eng.* 2024;09544089241271866.
- [25] Madhu J, Madhukesh JK, Sarris I, Prasannakumara BC, Ramesh GK, Shah NA, et al. Influence of quadratic thermal radiation and activation energy impacts over oblique stagnation point hybrid nanofluid flow across a cylinder. *Case Stud Therm Eng.* 2024;60:104624.
- [26] Shaheen A, Muhammad Hussain S, Ghazwani HA, Huma Z, Siddique I. Analytical solution of non-Newtonian Williamson fluid under the effect of magnetohydrodynamics. *Mod Phys Lett B.* 2024;38(13):2450103.
- [27] Shaheen A, Siddique I, Huma Z, Ahsan M, Khalid Z. Comparative analysis of viscous dissipation effects on Prandtl fluid including contraction and relaxation phenomena. *Heat Transf.* 2024;53(7):3687–705.
- [28] Afridi MI, Khan MS, Qasim M, Chamkha AJ. Computational analysis of unsteady oscillatory flow of nanofluid with variable electric conductivity: gear-generalized differential quadrature approach. *J Comput Des Eng.* 2024;11(6):20–35.
- [29] Mushahary P, Ontela S. Entropy analysis of mixed convective electro-magnetohydrodynamic couple-stress hybrid nanofluid flow with variable electrical conductivity in a porous channel. *Phys Scr.* 2024;99(11):115253.
- [30] Reddy YM, Ganteda C, Sreedhar S, Himabindu IBN, Sulaiman TA, Obulesu M, et al. Impact of variable electrical conductivity, viscosity on convective heat and mass transfer flow of CuO-and Al₂O₃-water nanofluids in cylindrical annulus. *Mod Phys Lett B.* 2024;39:2450425.
- [31] Hayat AU, Ahmad H, Gana S, Muhammad T, Eladeb A, Kolsi L. Entropy analysis in tri-hybrid nanofluid flow past a curved surface with applications of heat radiation and Lorentz force; numerical simulation. *J Radiat Res Appl Sci.* 2025;18(1):101276.
- [32] Gireesha BJ, Anitha L. Impact of shape dependent ternary hybrid nanofluid flow through a microchannel with quadratic thermal radiation: Irreversibility analysis. *J Appl Comput Mech.* 2024;10(4):729–41.
- [33] Gireesha BJ, Anitha L. Convective flow of couple stress ternary nanofluid flow through a permeable microchannel: irreversibility analysis. *Int J Model Simul.* 2024;1–18.
- [34] Hayat T, Naz S, Alsaedi A, Momani S. Melting and dissipative effects about entropy induced Darcy-Forchheimer flow involving ternary-hybrid nanofluids. *Case Stud Therm Eng.* 2024;55:104097.
- [35] Hayat AU, Khan H, Ullah I, Ahmad H, Alam MM, Bilal M. Numerical exploration of the entropy generation in tri-hybrid nanofluid flow across a curved stretching surface subject to exponential heat source/sink. *J Therm Anal Calorim.* 2024;149:1–13.
- [36] Liang R, Hanif H, Song J, Alzahrani SS. Heat transfer and entropy generation analysis of ternary nanofluid. *J Comput Des Eng.* 2024;11:qwae100.
- [37] Khan D, Kumam P, Watthayu W, Jarad F. Exploring the potential of heat transfer and entropy generation of generalized dusty tetra hybrid nanofluid in a microchannel. *Chin J Phys.* 2024;89:1009–23.
- [38] Ali F, Loganathan K, Eswaramoorthi S, Prabu K, Zaib A, Chaudhary DK. Heat transfer analysis on carboxymethyl cellulose water-based cross hybrid nanofluid flow with entropy generation. *J Nanomater.* 2022;2022(1):5252918.
- [39] Anitha L, Gireesha BJ. Irreversibility analysis of ternary hybrid nanofluid flow through an oblique microchannel with Hall current: a comparative study. *Int J Ambient Energy.* 2024;45(1):2355568.
- [40] Sohut FH, Khan U, Ishak A, Soid SK, Waini I. Mixed convection hybrid nanofluid flow induced by an inclined cylinder with Lorentz forces. *Micromachines.* 2023;14(5):982.
- [41] Zainal NA, Nazar R, Naganthran K, Pop I. MHD mixed convection stagnation point flow of a hybrid nanofluid past a vertical flat plate with convective boundary condition. *Chin J Phys.* 2020;66:630–44.
- [42] Rafique K, Mahmood Z, Adnan, Khan U, Farooq U, Emam W. Computational analysis of MHD hybrid nanofluid over an inclined cylinder: Variable thermal conductivity and viscosity with buoyancy and radiation effects. *Mod Phys Lett B.* 2024;39:2550033.